Journal of Material Sciences & Engineering

Research Article **Open Access**

Phase Formation in the Region of laser Irradiation of $Al_2O_3 - TiO_2 - Y_2O_3$ Oxide Eutectic Mixtures

Vlasova M[1], Márquez Aguilar PA[1]*, Kakazey M[1], Stetsenko V[2], Ragulya A[2] and Bykov A[2]

[1]Center of Investigation in Engineering and Applied Sciences of the Autonomous University of the State of Morelos, Universidad, Cuernavaca, Mexico
[2]Institute for Problems of Materials Science, National Academy of Sciences of Ukraine, Krzhyzhanovsky St, Ukraine

Abstract

The phase formation processes in the zone of directional laser irradiation of compacted Al_2O_3–TiO_2–Y_2O_3 mixtures have been investigated. It has been established that the formed ceramic material (track) has a complex structure. Its surface layer contains α-Al_2O_3 as the main phase and $Y_2Ti_2O_7$ inter layers. With increase in the distance from the surface of the track, the content of α-Al_2O_3 decreases, and the content of $Y_2Ti_2O_7$ increases. The volume layers of the track contain $Y_2Ti_2O_7$ as the main phase and inclusions of $Y_3Al_5O_{12}$. The absence of Al_2TiO_5 or its small content is explained by the decomposition of aluminum titanate into Al_2O_3 and TiO_2 under the conditions of rapid cooling of eutectic melt. Released titanium oxide takes part in the formation of the $Y_2Ti_2O_7$ phase.

Keywords: Al_2O_3–TiO_2–Y_2O_3 mixtures; Laser treatment; Phase formation

Introduction

Laser synthesis of ceramics from powder mixtures is a promising method for the preparation of materials with a complex of new properties that form under conditions of directional high-rate heating and subsequent high-rate cooling. This synthesis is characterized by the fact that phase formation proceeds in an arrow irradiation zone and is determined by the irradiation mode, thermal conductivity of the material, its thermal diffusivity, and a number of other technological factors [1-6]. This is why the considered method was called Selective Laser Synthesis (SLS), Though, as a rule, it is combined with selective laser sintering (denoted by the same abbreviation SLS) [7-9]. Selective laser sintering, in turn, is often combined with Selective Laser Melting (SLM) [9-12]. The complexity and short time of processes proceeding in the irradiation zone call for investigations that will enable one to separate (at least, at a first approximation) sintering processes from melting and phase formation processes. This problem is most urgent in the case where the result of irradiation is formation of interaction products. For instance, in [4,11], it was shown that the synthesis zone should be considered as a set of layers of different phase composition. In the direction, perpendicular to surface, the melting–crystallization zone (surface layer), sintering zone (lower layer), and transient zone between them can be distinguished. Correspondingly, each zone is characterized by its own mechanisms of phase formation and set of phases. As a rule, in the process of high-temperature heating of the surface and irradiated compact (up to 2000°C and over), along with the formation of new phases, the development of ablation processes and decomposition of primary and newly formed compounds occur. This, in turn must lead to a change in the phase composition of the surface layer and the development of new mechanisms of phase formation differing from those proceeding in the case of traditional methods of heating and cooling. Under conditions of directional laser irradiation, when the directional melting-solidification process of the surface layer is realized, emerging texturing effects lead to the additional modification of the surface properties of the irradiation zone (track). At present, the laser texturing of the surface of the ceramics of simple and complex composition is being extensively investigated and used. A relation between the irradiation mode, texturing character, and strength properties of the material was established [13,14]. However, the character of texturing in the zone of laser synthesis has not been adequately studied.

The aim of the present work is to investigate phase formation and the morphology of the surface in the zone of laser treatment of ternary (Al_2O_3–TiO_2–Y_2O_3) powder mixture. The interest to this ternary system is due to a number of causes. Binary mixtures based on these oxides have eutectic compositions [15]. Therefore, under directional laser irradiation, in the surface layer of compacted powder mixtures, eutectic melts must also form, and, in cooling, new compounds with texture elements must solidify. In this case, the features of phase formation in different temperature zones, particularly, in the melting-ablation zone, are of interest.

Experimental Procedure

In the present work, specimens were prepared from analytically pure Al_2O_3, TiO_2, and Y_2O_3 powders (produced by REASOL).

Powder mixtures x mol.% Al_2O_3-y mol% TiO_2–z mol.% Y_2O_3 were homogenized in a ball mill for 4 hours and then were compacted in pellets with a diameter of 18 mm and a thickness of 2-3 mm under a unidirectional pressure (axial pressure) of 300 MPa. The compositions of compacts are presented in Table 1. The compositions of the mixtures were calculated so that, with increased in the Al_2O_3 content in the mixture, the Y_2O_3/TiO_2 molar ratio will be $R≈0.35$ in specimens No. 1 and No. 3 and $R≈0.71$ in specimens No 3 and No 4.

Laser treatment was performed in an LTN-103 unit (continuous-action laser with λ=1064 nm). The power of radiation (P) was 120 W, the diameter of the beam (d) was 1.5 mm, and the linear traversing speed of the beam was v=0.15mm/s. A simplified scheme of irradiation

Number of the compact and track	Composition of the compact	Phase composition of the track*
1	63.5 mol.% Al_2O_3 + 27 mol.% TiO_2+ 9.5 mol.% Y_2O_3	$Y_2Ti_2O_7$, α-Al_2O_3, $Y_3Al_5O_{12}$, little β-Al_2TiO_5
3	77.7 mol.% Al_2O_3 +16.5 mol.% TiO_2 + 5.8 mol.% Y_2O_3	α-Al_2O_3, $Y_2Ti_2O_7$, little $Y_3Al_5O_{12}$, traces of β-Al_2TiO_5,
2	67.4 mol.% Al_2O_3 +19.1 mol.% TiO_2 + 13.5 mol.% Y_2O_3	$Y_2Ti_2O_7$, α-Al_2O_3, $Y_3Al_5O_{12}$
4	84.6 mol.% Al_2O_3 + 9.0 mol.% TiO_2 + 6.4 mol.% Y_2O_3	α-Al_2O_3, $Y_2Ti_2O_7$, $Y_3Al_5O_{12}$

*Note: phases are enumerated in the order of decrease in their content.

Table 1: Phase composition in zone of a track.

is shown in Figure 1a.

As a result of irradiation, concave channels (tracks) formed on the surfaces of specimens (Figure 1d). Their formation is associated with high temperatures in the irradiation zone, due to which the sintering and melting–solidification processes proceed simultaneously. These tracks were easily removed from the compacts (Figure 1b,c). The lower sides of the tracks were cleaned from the loose slightly sintered powder. The designations of tracks correspond to the designations of used mixtures.

The synthesis products were investigated by the X-ray Diffraction (XRD) method in Cu K_a radiation (a DRON-3M diffractometer, Russia). An electron microscopy study and an Electron-Probe Microanalysis (EPMA) were performed with a HU-200F type scanning electron microscope and a LEO 1450 VP unit. An Atomic Force Microscopy (AFM) investigation (Digital Instruments Nanoscope IV in tapping mode with a silicon nitride tip) was carried out in phase regime.

Results

XRD data

In the zone of laser irradiation of different mixtures, composite ceramic materials usually form (Figure 2 and Table 1). In tracks of specimens, No. 1 and No. 3, the α-Al_2O_3 and $Y_2Ti_2O_7$ crystal phases are dominant. The $Y_3Al_5O_{12}$ and β-Al_2TiO_5 phases form in much smaller amounts. In specimens' No. 2 and No. 4, α-Al_2O_3 and $Y_2Ti_2O_7$ also dominate, whereas β-Al_2TiO_5 is absent. In tracks with the same value of R, with increase in the Al_2O_3 content in the initial mixtures, the intensity of the lines of corundum increases, and the intensities of the lines of $Y_3Al_5O_{12}$ and $Y_2Ti_2O_7$ decrease (Figure 3). With change in the contents of TiO_2 and Y_2O_3 and their ratios, the intensities of the lines of phases containing Ti and Y change. In Figure 3, it is seen that the larger R, the higher the intensities of $Y_2Ti_2O_7$ and $Y_3Al_5O_{12}$. The formation of the $Y_2Ti_2O_7$ phase is preferred.

The deviation of the intensities of the lines of Al_2O_3 from standard values [16], indicates the texturing of corundum. In Table 2, the values of the Texture Coefficients (TC) for different phases in tracks Nos. 1-4 are presented. The calculation was performed by the formula [17]

$$TC(hkl) = \frac{I(hkl)}{I_o(hkl)} \left\{ \frac{1}{n} \sum \frac{I(hkl)}{I_o(hkl)} \right\}^{-1},$$

where I(hkl) are the measured intensities of the (hkl) reflection, I_o(hkl) are the calculated intensities presented in the JCPDS cards, and n is the number of reflections used in the calculation. In the calculation, cards No. 83-2080 for α-Al_2O_3, No. 89-2065 for $Y_2Ti_2O_7$, and No. 82-0575 for $Y_3Al_5O_{12}$ were used [16].

It follows from Table 2 and Figure 4a that the texturing of α-Al_2O_3 crystallites occurs in the direction <1010>. Their Texture Coefficient (TC) decreases as the Al_2O_3 content in the initial mixtures increases. The tendency of the dependence of the TC on the Al_2O_3 content in the initial mixtures is also observed for the $Y_3Al_5O_{12}$ phase in the direction <840>. However, for the $Y_2Ti_2O_7$ phase, the change (increase) in the TC correlates with the decrease in the Y_2O_3 content in the directions <444> and <800> (Figure 4b).

Electron microscopy and EPMA data

The surface of the track formed in irradiation of mixture No. 1 has a complex texture. On its surface, we can see macro texture in the form of arcs (Figure 5a), which reflects the motion stage of the solidifying melt under the action of the traversing laser beam. Arcs consist of accumulations of particles (domains). Domains can be considered as elements of microtexture (Figure 5b). In the micrograph of a diagonal section of a track (Figure 5c), it is seen that the upper part of the track consists of predominantly dark crystallites, between which light interlayers are present. The EPMA data indicate (Figure 5e) that the domains on the surface of the track and dark crystallites (Figure 5c) contain primarily Al and O. In the composition of interlayers, along with Al and O, the presence of Y and Ti was registered. In the cross-section of the track, in the sintering zone (Figure 5d), the inhomogeneity of distribution of the newly formed compounds and Al_2O_3 is observed. This is the result of the crystallization behavior of the heterophase
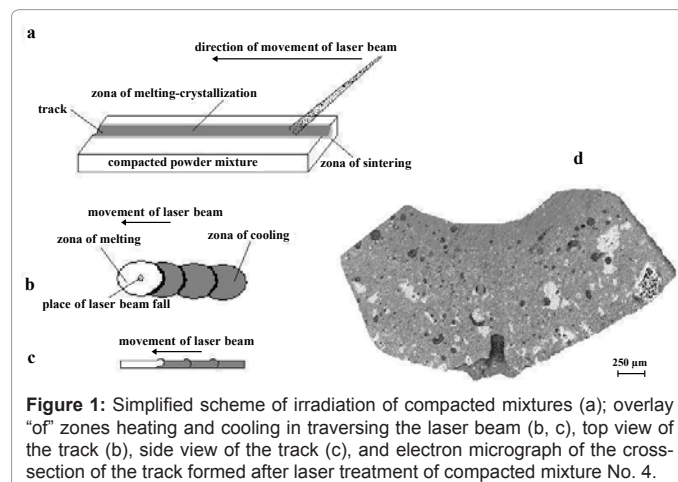
Figure 1: Simplified scheme of irradiation of compacted mixtures (a); overlay "of" zones heating and cooling in traversing the laser beam (b, c), top view of the track (b), side view of the track (c), and electron micrograph of the cross-section of the track formed after laser treatment of compacted mixture No. 4.

Figure 2: Fragments of X-ray diffraction patterns of tracks. (a) in tracks No. 1 and No. 3; (b) in tracks No. 2 and No. 4. (●) α-Al_2O_3; (β) β-Al_2TiO_5; (v) $Y_2Ti_2O_7$; (x) $Y_3Al_5O_{12}$.

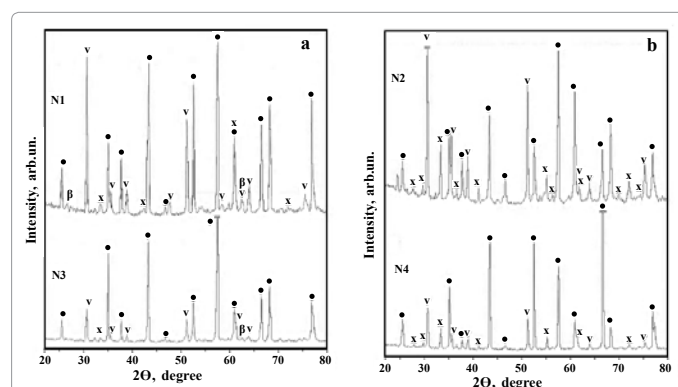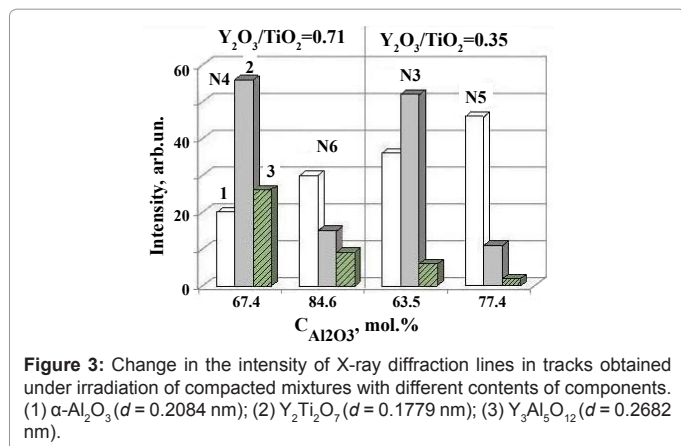**Figure 3:** Change in the intensity of X-ray diffraction lines in tracks obtained under irradiation of compacted mixtures with different contents of components. (1) α-Al_2O_3 (d = 0.2084 nm); (2) $Y_2Ti_2O_7$ (d = 0.1779 nm); (3) $Y_3Al_5O_{12}$ (d = 0.2682 nm).

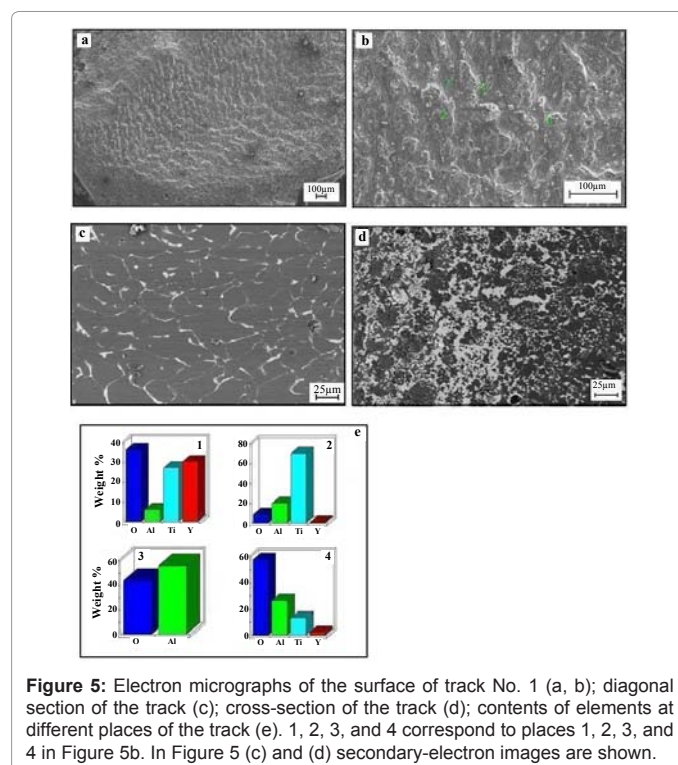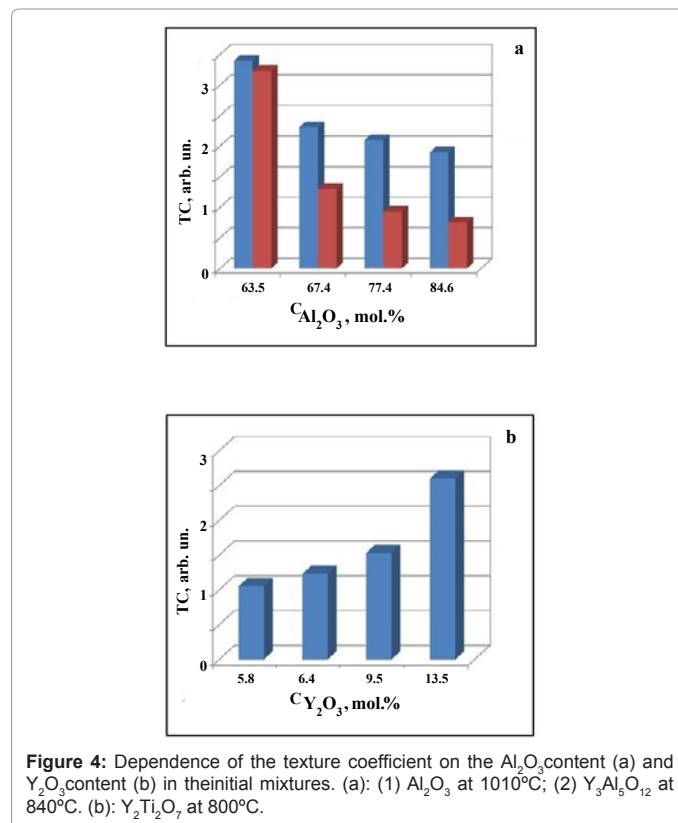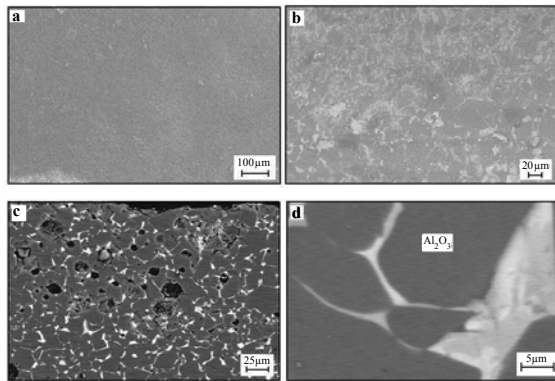| Phase	Number of the track	C_{Al2O3}, mol. %	TC for [hkl]							
			104	110	113	024	116	214	300	1010
α-Al_2O_3	No. 1	63.5	0.32	0.54	0.7	1.2	0.8	1.1	0.94	**3.4**
	No. 2	67.4	0.48	0.67	0.66	0.9	1.25	1.2	1.1	**2.31**
	No. 3	77.7	0.68	1.49	0.8	0.6	1.25	0.97	0.81	**2.1**
	No. 4	84.6	0.42	0.1	0.78	1.6	0.62	**3.1**	0.3	1.9
	Number of the track	C_{TiO2}, mol. %	331	440	444	800	622			
$Y_2Ti_2O_7$	No. 1	27.0	0.48	0.66	**1.74**	1.53	0.85			
	No. 2	19.1	0.82	0.66	0.66	**2.06**	0.93			
	No. 3	16.5	0.59	0.68	0.13	1.05	1.32			
	No. 4	9.0	0.58	0.64	1.34	1.23	1.01			
	Number of the track	C_{Al2O3}, mol. %	521	640	840	842				
$Y_3Al_5O_{12}$	N 1	63.5	0.8	0.32	**3.23**	0.32				
	N 2	67.4	0.7	1.06	1.3	1.4				
	N 3	77.7	0.64	1.23	0.93	1.43				
	N 4	84.6	0.56	1.5	0.75	1.5				

Table 2: Values of the texture coefficients in tracks.

material, which is characterized by the substantial difference between the melting points of the phases present in it.

As the Al_2O_3 content in the mixture increases (mixture No. 3), the surface of the track changes substantially. The macro and micro texture are less pronounced (Figure 6a). Corundum crystallites and thin interlayers between them form a "reticular" structure on the surface of the track (Figure 6a, 6b). As is seen in Figure 6d, a part of interlayers consist of regions of different color (gray and light-gray). This means that they have a complex phase composition. Taking into account the X-ray diffraction data, we can state that they contain $Y_2Ti_2O_7$ and $Y_3Al_5O_{12}$. This is substantiated by the EPMA data. In a fracture of a specimen (Figure 7a), between large crystallites containing Al and O (Figure 7b), fine grains containing Al, O, Ti, and Y are present. With decrease in the distance to the surface, the interlayers between corundum grains become thinner (Figure 6c).

The morphology of the surface of tracks, No. 2 and No. 4, is similar to that for specimen No. 3 (Figure 8a, 8b and Figure 9b). On the rough surface of the tracks, arc-shaped "beads" are observed (Figure 8c and Figure 9b, 9c). They consist of aggregates of particles (Figure 9d) and the material crystallized in the form of tourniquets/lamellas (Figure 9c). The EPMA data indicate that Al and O dominate in aggregates of particles (domains) and that Al, O, Ti, and Y dominate in lamellas

(Figure 9c, 9d and Figure 10). The inhomogeneity of distribution of the elements in the direction from the surface of the track to the sintering zone (Figure 9e, 9f and Figure 11 a,11b) also reveals the predominance of Al and O on the surface of the track. Correspondingly, with decrease

Figure 4: Dependence of the texture coefficient on the Al_2O_3content (a) and Y_2O_3content (b) in theinitial mixtures. (a): (1) Al_2O_3 at 1010°C; (2) $Y_3Al_5O_{12}$ at 840°C. (b): $Y_2Ti_2O_7$ at 800°C.

Figure 5: Electron micrographs of the surface of track No. 1 (a, b); diagonal section of the track (c); cross-section of the track (d); contents of elements at different places of the track (e). 1, 2, 3, and 4 correspond to places 1, 2, 3, and 4 in Figure 5b. In Figure 5 (c) and (d) secondary-electron images are shown.
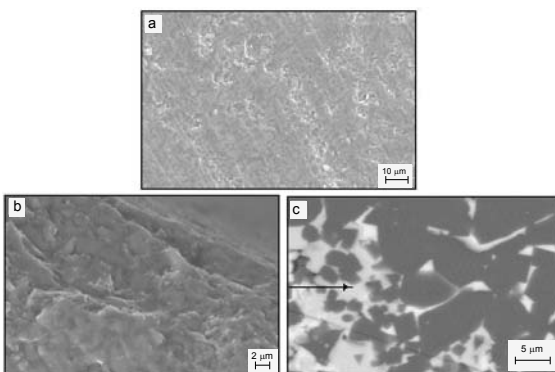
Figure 6: Electron micrographs of the surface of track No. 3 (a, b) and its cross-section (c, d). In Fig. 6b, 6c, 6d, secondary-electron images are shown.
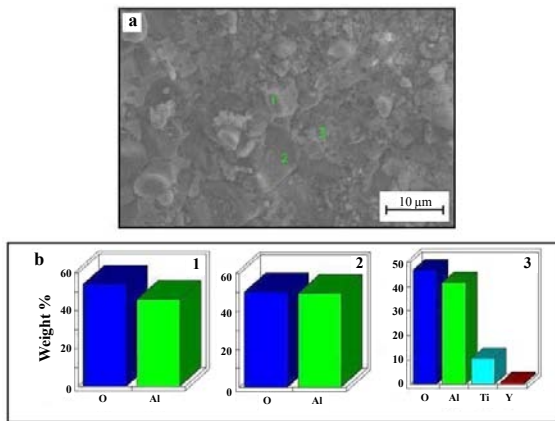
Figure 7: Electron micrographs of a fracture of track No. 3 (a) and the contents of elements at different places of the track (b). 1, 2, and 3 in (b) correspond to places 1, 2, and 3 in Figure 7a.

Figure 8: Electron micrographs of the surface of track No. 2 (a, b) at different magnifications and its cross-section (c). The arrow in Figure 8c indicates the direction to the surface of the track. In Figure 8c secondary-electron image is shown.

in the distance to the surface of the track, Al_2O_3 grains increase in size, and the thickness of the interlayers between them decreases (Figure 8d). With increase in the distance from the surface of the track (to the sintering zone), the thickness of interlayers between Al_2O_3 crystallites increases, and, along with Al and O, in the interlayers, Ti and Y are clearly identified (Figure 9f and 11). On the surface of the tracks,

"lamellas" which have the form of rapidly cooled melt, form (Figure 9e).

AFM data

The AFM investigation enabled us to detect the micro and nano texture of the surface of tracks. For instance, domains (aggregates of domains) of different size rise above the surface of the track (Figure 12a). Each domain element, in turn, consists of microparticles, which form chains of different length (Figure 12b). The size of nano particles in domains is about 14 nm. The surface above which domains rise is also the crystallized material composed of particles with a size of about 7 to 50 nm. They form structures of different directivity, namely, arcs and chains of different height and width (Figures 12a, 12d).
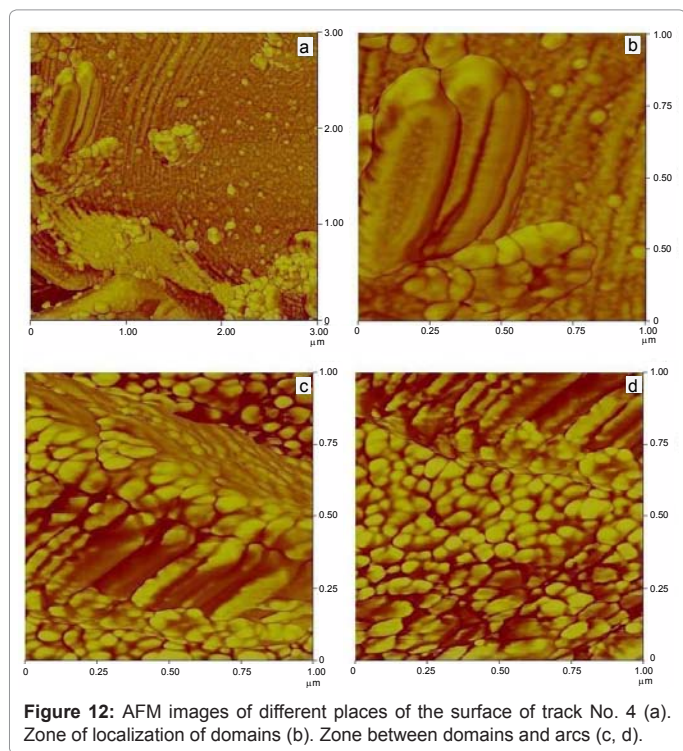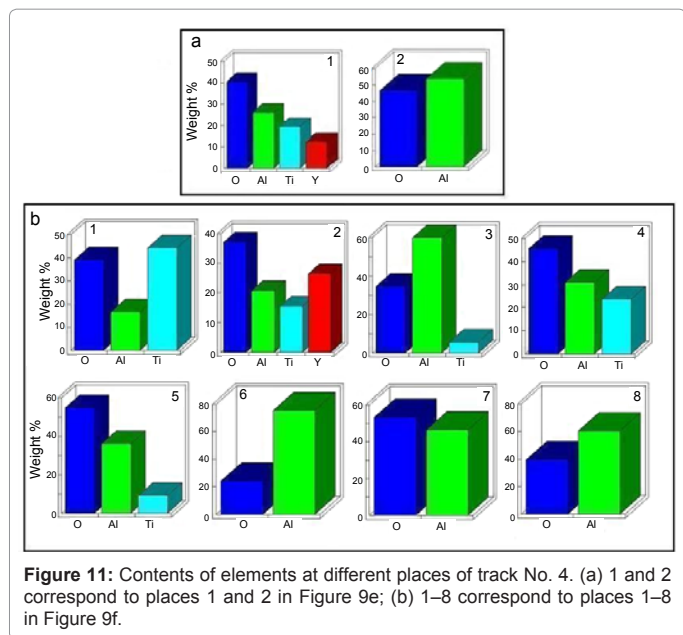
According to the SEM and EPMA data, domains on AFM images can be assigned to Al_2O_3. As a rule, elements that correspond to the formation of ternary compounds are recorded between arcs and in lamellas. For this reason, arc-shaped aggregates of particles and lamellas on AFM images can be considered as places of localization of $Y_2Ti_2O_7$ and $Y_3Al_5O_{12}$. In Figure 9c, done can see places of superposition
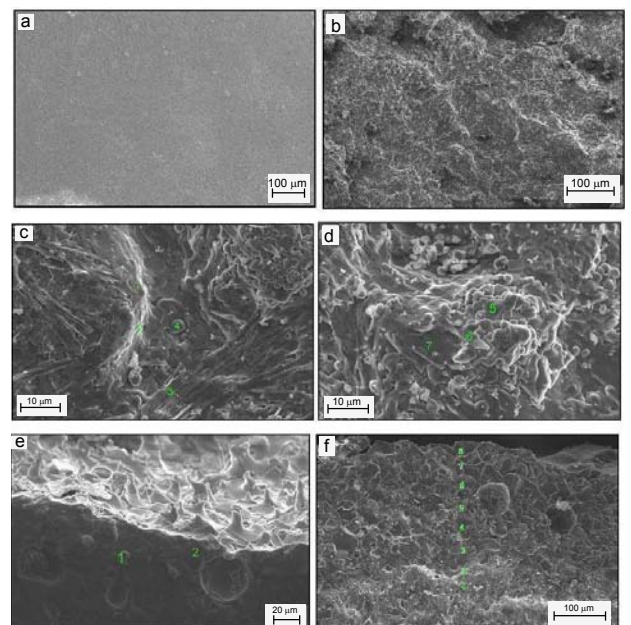
Figure 9: Electron micrographs of the surface of track No. 4 (a, b, c, d), on the boundary of a fracture (e), and on the fracture of the track (f). In Figure 9f secondary-electron image is shown.
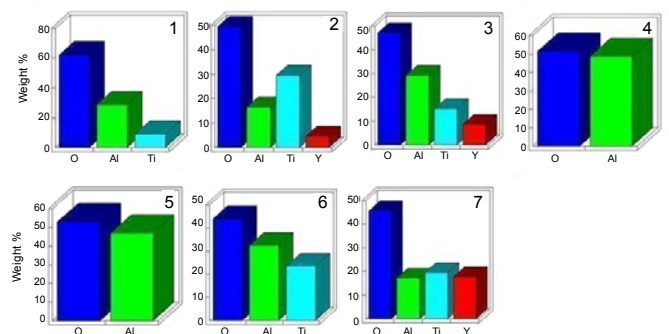
Figure 10: Contents of elements at different places of the surface of track No. 4. (a) 1–7 correspond to places 1–7 in Figure 9c, 9d.

Figure 11: Contents of elements at different places of track No. 4. (a) 1 and 2 correspond to places 1 and 2 in Figure 9e; (b) 1–8 correspond to places 1–8 in Figure 9f.

Figure 12: AFM images of different places of the surface of track No. 4 (a). Zone of localization of domains (b). Zone between domains and arcs (c, d).

of layers with different degrees of texturing and different directions of texturing. This effect is due to the movement of the melt in traversing the laser beam.

Discussion

In choosing the composition of x mol.% Al_2O_3–y mol.% TiO_2, x mol% Al_2O_3–y mol.% Y_2O_3, or x mol% TiO_2–y mol% Y_2O_3 binary powder mixture and heat treatment conditions, it is rather easy to predict the phase composition of compounds that precipitate from the cooled eutectic melt [15]. However, in view of the complexity of homogenization of powder mixtures and the heterogeneity of the

temperature distribution in compacts in the irradiation zone, for x mol.% Al_2O_3–y mol.% TiO_2–z mol.% Y_2O_3 ternary mixtures, the phase formation process must have a complex character, and the track material must consist of a set of local phases that form in local temperature zones.
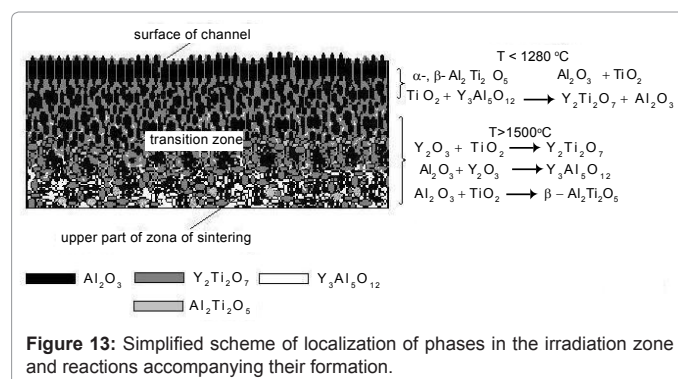
In analyzing the obtained results, the following facts attracted our attention. In tracks, Al_2O_3 and $Y_2Ti_2O_7$ are dominant among crystalline phases. Yttrium titanate forms even in the case where the contents of TiO_2 and Y_2O_3 in the mixtures are insignificant. As the Al_2O_3 content in the mixtures increases, the crystallization of corundum dominates, and the formation of $Y_3Al_5O_{12}$ and Al_2TiO_5 is suppressed in the tracks (Figure 3). This enables us to assume that the eutectic melt is enriched in TiO_2 and Y_2O_3, which provides more favorable conditions for the formation of $Y_2Ti_2O_7$.

In the direction from the sintering zone to the surface of the track (in the vertical direction), the microstructure of the track changes through stages of formation of individual eutectic zones (Figure 5d) to the matrix structure (see Figure 8d), in which the content of the main $Y_2Ti_2O_7$ phase gradually decreases, and Al_2O_3 becomes the main phase (Figs 5c, 6d, 8d). In this direction, the growth of corundum grains and a decrease in the thickness of inter layers between them occur. As a result, the total content of the $Y_2Ti_2O_7$ and $Y_3Al_5O_{12}$ in the surface layer of the track decreases. For this reason, the intensity of the lines of the indicated phases in the X-ray diffraction patterns decreases substantially (Figure 3).

The traversing of the laser beam over the surface of the compact initiates not only high-temperature melting of the surface layer of the compact, but also its rapid cooling. As the heating zone shifts, the partial overlap of layers and the motion of the viscous material take place (Figure 9b, 9c, 9e), namely, a new portion of the melt is ejected onto the cooled melt in the horizontal direction (Figure 1b,1c). This leads to both the formation of "combs" on corundum domains extending above the surface and the "corrugating" effect of cooling and solidifying eutectic melt of different of viscosity (Figure 9e, Figure 12a, and Figure 1b, c).

The decrease in the texture coefficient of α-Al_2O_3 with increasing aluminum oxide content in the mixtures and its transformation into the main phase (Table 2) can be explained by the conflict of growth of corundum crystals in a certain predominant direction during rapid solidification of the melt. Analogous conditions are realized for the texturing of $Y_3Al_5O_{12}$ and $Y_2Ti_2O_7$. For these phases, the texture was found to be more pronounced in the case where $Y_2Ti_2O_7$ is the matrix phase, i.e., at a small α-Al_2O_3 content.

Since the main newly formed compounds belong to phases of

Figure 13: Simplified scheme of localization of phases in the irradiation zone and reactions accompanying their formation.

binary systems, the characteristic features of their formation under the conditions of heterogeneity of the mixtures and a temperature gradient in the vertical and radial directions should be noted. The compounds $Y_2Ti_2O_7$, $Y_3Al_5O_{12}$, and β-Al_2TiO_5 must form at contact points of particles and aggregates of the corresponding oxides at the corresponding local concentration ratios of the components in a certain temperature zone. The upper limiting temperature of existence ranges from 1820 to 1700°C for β-Al_2TiO_5 at different concentrations and is equal to 1820°C for $Y_3Al_5O_{12}$. The lower limiting temperature of their synthesis ranges from ~1280 to ~1350°C [18-22]. These conditions are satisfied in the low-temperature irradiation zone, i.e. the sintering zone.

For the formation of $Y_2Ti_2O_7$ in the contact zone of Y_2O_3 and TiO_2 particles, higher temperatures (T>1500°C) and larger treatment times (several hours) are required [23,24]. Only at high heating temperatures, the time of formation of yttrium titanate can be decreased. The temperatures obtained on the surface of compacts correspond to these conditions.

According to the Al_2O_3–TiO_2 constitution diagram, at high temperatures (in the surface layer of the track), α-Al_2TiO_5 must form. Under conditions of rapid cooling, at T<1280°C, it must decompose into α-Al_2O_3 and TiO_2 (rutile) (eutectoid decomposition) [25]. In this case, the surface layer must be enriched in aluminum oxide, and the freed titanium oxide can take part in the formation of $Y_2Ti_2O_7$ as a result of the interaction of TiO_2 with both Y_2O_3 and $Y_3Al_5O_{12}$ [26]. This is why, in the X-ray diffraction patterns, rutile lines are absent.

In cooling the melt, $Y_2Ti_2O_7$ and $Y_3Al_5O_{12}$ crystallize at temperatures lower than the crystallization temperature of Al_2O_3. In this case, in the surface layer, conditions of emergence of α-Al_2O_3 nuclei, their growth, and displacement of the $Y_2Ti_2O_7$+$Y_3Al_5O_{12}$ melt into volume layers of the track dominate. For this reason, predominantly Al and O are detected in the surface layer, and the contents of Y and Ti increase in volume layers (Figure 5c, Figure 9f, and Figure 11b). We believe that this mechanism of displacement of the melt by growing corundum crystals eventually leads to the transformation of the leading main phases.

In the intermediate temperature zone, local eutectics gradually transform into a homogenized eutectic (towards the surface). However, it can be assumed that, due to the displacement of the heating zone and further rapid cooling, eutectic melts have no time to be homogenized (Figure 6d).

Thus, in the laser irradiation zone, tracks with a gradually varying phase composition form. Their composition is determined by not only the temperature gradient and heterogeneity of the mixture, but also a series of reactions that proceed in the high-temperature region and under conditions of rapid heating and cooling. In Figure 13a simplified scheme of the structure of a track is shown.

Conclusions

The performed investigations have shown that, in the zone of laser treatment, phase formation processes characteristic for different temperature zones, proceed:

- In the low-temperature heating zone adjacent to the sintering region, eutectic melts forming the contact regions of particles and aggregates of binary mixtures due to the heterogeneity of mixtures and the presence of a temperature gradient in the axial direction
- In the high-temperature heating regions, the formation of the TiO_2–Y_2O_3 eutectic is intensified
- In passing from the low-temperature heating zone, in which the

$Y_2Ti_2O_7$ phase is matrix, to the high-temperature heating zone, its content decreases, and α-Al_2O_3 becomes the matrix phase
- The absence of Al_2TiO_5 in the ceramic tracks can be associated with its decomposition into Al_2O_3 and TiO_2 under the conditions of rapid cooling
- The absence of TiO_2 in the ceramic tracks is explained by its participation in the formation of $Y_2Ti_2O_7$
- The directed motion of the eutectic melt on the surface of the tracks influences the texturing of the surfaces of the tracks
- The degree of texturing of α-Al_2O_3, $Y_2Ti_2O_7$, and $Y_3Al_5O_{12}$ crystallites in the tracks depends on the volume ratio of the matrix phase and secondary phases.

References

1. Sugihara S, Fukuyama T (1992) Synthesis of electronic ceramics by using CO_2 laser. Ferroelectrics 133: 307-311.

2. Xingjiao L, Fang Z, Qiguang Z, Jiarong L, Zaiguang L, et al. (1993) Analysis of aluminum tungsten oxide ceramics synthesized by a high-power cw CO_2 laser. J Appl Phys 74: 1616-1624.

3. Shishkovsky I, Yadroitsev I, Bertrand Ph. Smurov I (2007) Alumina–zirconium ceramics synthesis by selective laser sintering/melting. Appl Surf Sci 254: 966-970.

4. Heinrich JG, Gahler A, Gunster J, Schmucker M, Zhang J, et al. (2007) Microstructural evolution during direct laser sintering in the Al_2O_3–SiO_2 system. J Mater Sci 42: 5307-5311.

5. Gahler A, Heinrich JG, Gunster J (2006) Direct Laser Sintering of Al_2O_3–SiO_2 Dental Ceramic Components by Layer-Wise Slurry Deposition. J Am Ceram Soc 89: 3076-3080.

6. Kakazey M, Vlasova M, Márquez Aguilar PA, Bykov O, Stetsenko V, et al. (2009) Laser Surface Solutionizing and Crystallization of Al_2O_3–Cr_2O_3. International Journal of Applied Ceramic Technology 6: 335-343.

7. Shishkovskii IV (2009) Laser synthesis of functional mesostructures and 3D parts. Fizmatlit, Moscow.

8. Kruth JP, Wang X, Laoui T, Froyen L, (2003) Lasers and materials in selective laser sintering. Assembly Autom 23: 357-371.

9. Sikalidis C (2011) Advances in Ceramics - Synthesis and Characterization, Processing and Specific Applications. InTech-Open Access, USA.

10. Kruth JP, Mercelis P, Vaerenbergh JV, Froyen L, Rombouts M (2005) Binding mechanisms in selective laser sintering and selective laser melting. Rapid Prototyping Journal 11: 26-36.

11. Vlasova M, Kakazey N, Márquez Aguilar PA, Stetsenko V, Ragulya A (2010) Laser horizontally directed synthesis of ruby. Superficies y Vacio 23: 15-20.

12. Averyanova M, Bertranda Ph, Verquinb B (2011) Studying the influence of initial powder characteristics on the properties of final parts manufactured by the selective laser melting technology. Virtual and Physical Prototyping 6: 215-223.

13. Berger MH, Sayir A (2008) Directional solidification of Al_2O_3–Al_2TiO_5 system. J Eur Ceram Soc 28: 2411-2419.

14. Orera VM, Merinoa RI, Pardoa JA, Larreaa A, Pena JI, et al. (2000) Microstructure and physical properties of some oxide eutectic composites processed by directional solidification. Acta Mater 48: 18-19.

15. Toropov NA (1969) Constitutional diagrams of silicate systems. Nauka, Leningrad.

16. JCPDS, Swarthmore, PA, 1996.

17. Ruppi S (2005) Deposition, microstructure and properties of texture-controlledCVD α-Al_2O_3 coatings. Int J Refract Met H 23: 306-316.

18. Sekar MMA, Patil KC (1994) Synthesis and properties of tialite, beta-Al_2TiO_5. Brit Ceram T 93: 146-149.

19. Freudenberg B, Mocellin A (1987) Aluminum Titanate Formation by Solid-State Reaction of Fine Al_2O_3 and TiO_2 Powders. J Am Ceram Soc 70: 33-38.

20. Somani V, Kalita SJ (2007) Synthesis, Densification, and Phase Evolution Studies of Al_2O_3-Al_2TiO_5-TiO_2 Nanocomposites and Measurement of Their Electrical Properties. J Am Ceram Soc 90: 2372-2378.

21. Veith M, Mathur S, Kareiva A, Jilavi M, Zimmer M, et al. (1999) Low temperature synthesis of nanocrystalline $Y_3Al_5O_{12}$ (YAG) and Ce-doped $Y_3Al_5O_{12}$ via different sol-gel methods. J Mater Chem 9: 3069-3079.

22. Harada Y, Uekawa N, Kojima T, Kakegawa K (2008) Fabrication of $Y_3Al_5O_{12}$-Al_2O_3 eutectic materials having ultra fine microstructure. J Eur Ceram Soc 28: 235-240.

23. Mizutani N, Tajima Y, Kato M (1976) Phase Relations in the System Y_2O_3-TiO_2. J Am Ceram Soc 59: 168.

24. Kato M, Kubo T (1967) Solid State Reaction in the System Y_2O_3 — TiO_2. J Chem Soc Jpn 70: 840-843.

25. Kato E, Daimon K, Kobayashi Y (1980) Decomposition Temperature of β-Al_2TiO_5. J Am Ceram Soc 63: 355-356.

26. Zhou Y, Yue Z, Li L (2010) Preparation and Microwave Dielectric Properties of TiO_2-Doped YAG Ceramics. Ferroelectrics 407: 69-74.